JOC The Journal of Organic Chemistry
Article
Cite This: J. Org. Chem. XXXX, XXX, XXX−XXX
pubs.acs.org/joc

Indole-Fused Acridone: Synthesis, Structures, Proton Transfer, and Hole-Transport Properties

Ying-ying Jin and Qi Fang*

State Key Laboratory of Crystal Materials, Shandong University, Jinan 250100, China

Supporting Information

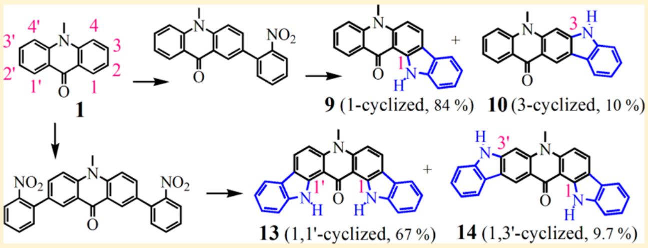

ABSTRACT: Three pairs of regioisomers of the planar acridone derivatives (**9** vs **10**, **11** vs **12**, and **13** vs **14**), classified as the 1-cyclized compounds (**9**, **11**, and **13**) and the 3-cyclized (or 1,3′-cyclized) regioisomers (**10**, **12**, and **14**), have been synthesized, and their X-ray structures have been determined. The 1-cyclized compounds have higher yields and lower energies compared with their 3-cyclized isomers. The fluorescence spectra of the intramolecular H-bond containing compounds (**9**, **11**, **13**, and **14**) consist of two bands (shorter wavelength band for the keto form and longer wavelength band for the enol form) and exhibit the feature of the excited-state intramolecular proton transfer (ESIPT). The density functional theory (DFT) theoretical investigation of the reorganization energy (λ) with respect to molecular symmetry revealed that planar rigid-C_{2v}-symmetric polycyclic heteroaromatic molecules (such as acridone, **1**, and **13**) can have low charge-transport barrier (small λ value) and keep the invariance of the molecular point group in the charge-transport process, and therefore can have high hole mobility.

INTRODUCTION

Since the appearance of the organic field-effect transistors (OFETs) 30 years ago,[1] high-performance organic semiconductor materials have acquired rapid progress as summarized in several reviews.[2−5] Designs and syntheses of new functional molecules are always the essential engines to promote the development of organic electronic materials. On the basis of novel compounds, numerous semiconductors with high charge-transport mobility (μ) have been reported in recent years.[6−17] The structure−property correlations of organic semiconductors can be focused on the following equation

$$\mu = \frac{e}{2k_BT\hbar}\left(\frac{\pi}{\lambda k_BT}\right)^{1/2} d^2t^2 \exp\left(-\frac{\lambda}{4k_BT}\right) \qquad (1)$$

which is based on the Marcus electron-transfer theory[18,19] and the well-known hopping model. In the mobility expression 1, λ is the reorganization energy and is the property of the molecule, and t is the transfer integral which is jointly dependent on the molecule and the intermolecular interactions in the crystal. Therefore, minimization of the λ is of the upmost importance in designing organic semiconductors at the molecular level and the λ can be quantum chemically predicted (vide infra).[20] When not specified, the calculations for λ, energies, and geometric optimizations in this work were carried out by the DFT/B3LYP/6-311g(d) methods. The λ is for the hole-transport process ($\lambda = \lambda_h$); if otherwise, for electron-transport process the reorganization energy will be denoted by λ_e.

Organic semiconductive compounds usually feature rigid geometry and highly π-conjugated structure, such as acenes and thienoacenes (see Table 1). We noticed that some semiconductive compounds take the C_{2v} molecular point group and have small λ values, such as dibenzo[*d*,*d*′]thieno[3,2-*b*;4,5-*b*′]dithiophene[21,22] (DBTDT, see Table 1) and dinaphtho[2,3-*b*:2′,3′-*d*]thiophene[23] (DNT, see Table 1).

To investigate the influence of symmetry on reorganization energy (λ), we carried out more λ-calculations for polycyclic aromatic and heteroaromatic molecules with different point groups and different π-dimensions. The λ values of the well-known D_{2h}-symmetric acenes are listed in the entry 1 of Table 1. If one central carbon atom of the above acenes was replaced by a nitrogen atom, the resultant C_{2v}-symmetric compounds in the entry 2 of Table 1 would have smaller λ values. The comparison of the pairwise isomers of thienoacene compounds[5,24−26] in the entries 4 and 5 indicates that the C_{2v} compounds here are superior to their C_{2h} isomers. Some multilayer polycyclic aromatic and heteroaromatic compounds are collected in the entries 6 and 7, where the λ values of the C_{2v}-symmetric compounds 7-1 and 7-2 are about half of those of the similar π-dimensional D_{2h}- and C_{2h}-symmetric compounds in the entry 6 and the λ value of the biradical 7-3 is only a quarter of that of the similar π-dimensional ovalene.

Generally, extension of the π-conjugation tends to reduce the λ in acene system, such as the larger λ of anthracene and the smaller λ of tetracene (see Table 1). The same tendency was also reported for thienoacene system.[27] However, as

Received: November 19, 2018

DOI: 10.1021/acs.joc.8b02939
J. Org. Chem. XXXX, XXX, XXX−XXX

Table 1. Calculated Reorganization Energies (λ in meV) of Some Compounds with Various Molecular Point Groups by DFT/B3LYP/6-311g(d) Methods

1	D_{2h}	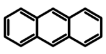 anthracene **137.0**	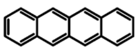 tetracene **114.0**	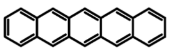 pentacene **97.9**	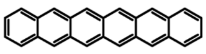 hexacene **85.6**	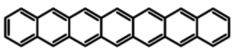 heptacene **75.8**	
2	C_{2v}	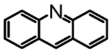 acridine: **135.5**	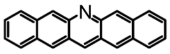 acridine-2[a]: **93.9**	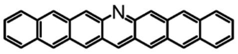 acridine-3[a]: **74.9**			
3		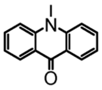 compd **1** C_s **71.5**	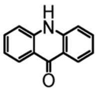 acridone C_{2v} **97.7**	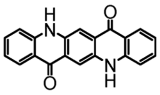 quinacridone C_{2h} **143.4**	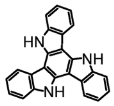 triindole[b] C_{3h} (C_s)	 coronene[b] D_{6h} (D_{2h})	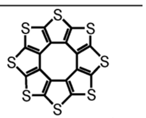 sulflower[b] D_{8h} (C_{2h})
4	C_{2h}	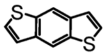 *anti*-BDT[24] **153.4**	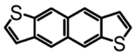 *anti*-NDT[5] **105.2**	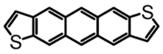 *anti*-ADT[25] **97.2**	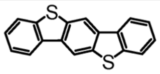 *anti*-BBBT[5] **94.9**		
5	C_{2v}	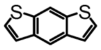 *syn*-BDT[24] **102.3**	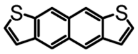 *syn*-NDT[5] **98.4**	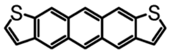 *syn*-ADT[26] **95.4**	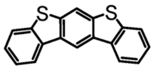 *syn*-BBBT **64.7**		
6	D_{2h} C_{2h}	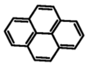 pyrene: **147.5**	 perylene: **145.6**	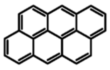 6-1: **115.7**	 6-2: **129.2**	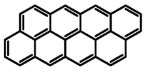 6-3: **92.0**	 ovalene: **93.8**
7	C_{2v}	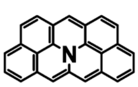 7-1[a]: **49.3**	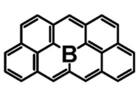 7-2[a]: **59.3** (λ_e)	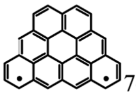 7-3[a,c]: **21.7**			
8	C_{2v}	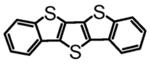 DBTDT: **83.7**	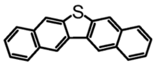 DNT: **112.4**	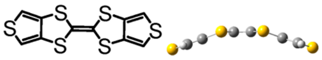 DT-TTF[b] C_{2v} (D_{2h})			

[a]Unknown compounds which cannot be found in the Web site of SciFinder. [b]The point groups in parentheses are of the cation. [c]The calculated triplet state of compound 7-3 is 0.81 eV lower than that of the singlet state.

shown in the entry 3 of Table 1, the λ value (97.7 meV) of the small-size C_{2v}-type acridone is much smaller than that (143.4 meV) of the large-size C_{2h}-type quinacridone, implying the advantage of the C_{2v} symmetry. For the synthetic facility, the N atom of acridone was methylated to improve solubility, and the point group of the resultant compound **1** (see Table 1) degenerates to C_s or quasi-C_{2v}. This methylation does not affect the molecular rigidity but further reduces the λ value (**1** vs acridone).

From syntheses and materials perspectives, acridone has good air and thermal stability and it can be easily modified. Up to now, reports about the syntheses and the charge-transport properties of π-fused acridone derivatives are very limited.[28−31] With the above ideas in mind, we synthesized π-extended C_s- or quasi-C_{2v}-symmetric compound **13** (see Scheme 1) by fusing two indole units to the parent compound **1**. The term quasi-C_{2v} symmetry for compounds **1** and **13** is based on the fact that their non-hydrogen molecular skeletons have C_{2v} symmetry. The λ value of compound **13** (105.3 meV) is between those of C_{2v}-type of DBTDT and DNT, implying that acridone derivatives may be a kind of potential organic semiconductive material. Herein, the syntheses, X-ray structures, photophysical properties, and theoretical hole-transporting behaviors of the series of indole-fused acridone compounds **9−14** (see Scheme 1) are reported.

■ RESULTS AND DISCUSSION

1. Syntheses of Compounds 9−14. We initially attempted to synthesize the precursor **8** of **13** by route 1 (see Scheme 1). However, after Suzuki coupling of 1 equiv of **3** and 4 equiv of 2-nitrophenylboronic acid, we isolated **7** instead of the expected **8**, together with the debromination compounds **1** and **2**. Presumably this failure should be caused by the strong electron-withdrawing effect of the nitro substituent.[32] Compound **7** was then treated with excess amount of PPh_3 in 1,2-dichlorobenzene (*o*-DCB)[33] at 180 °C for 36 h, obtaining 1-cyclized compound **11** and 3-cyclized compound **12,** which have been well-separated via silica gel chromatography.

To obtain compound **13,** we then designed route 2 shown in Scheme 1. First the dibrominated **3** was reacted with bis(pinacolato)diboron (B_2pin_2) to give **5** in 79% yield. After

Scheme 1. Synthetic Procedure for 9−14

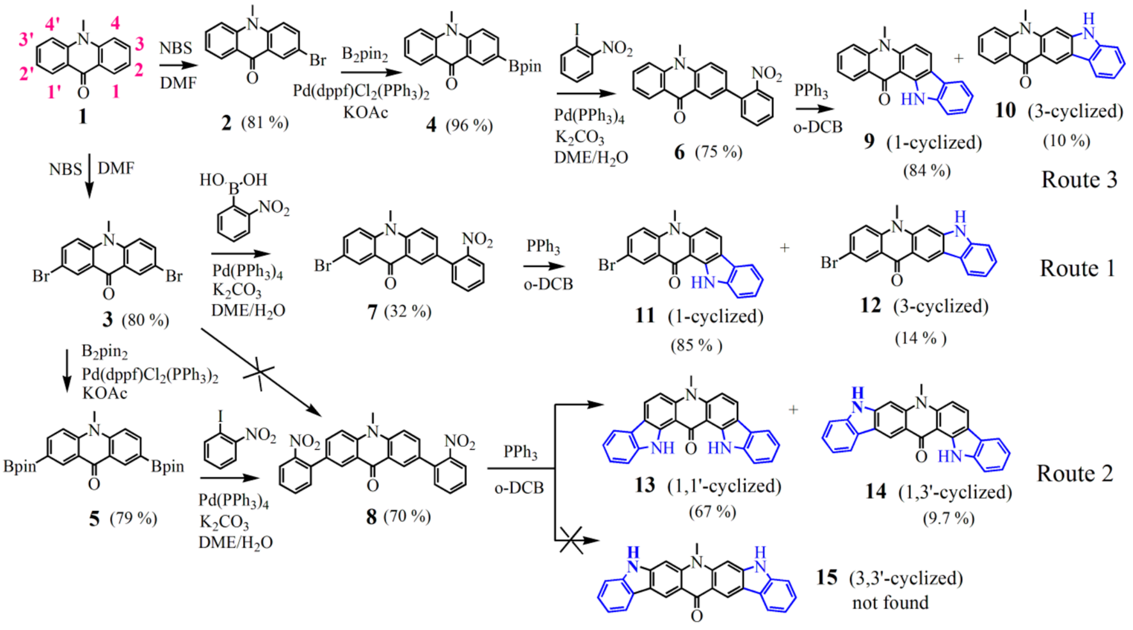

Suzuki coupling of **5** and 2-nitroiodobenzene, the precursor **8** was obtained in 70% yield. Then, treating **8** with excess amount of PPh_3 in *o*-DCB at 180 °C for 36 h, we finally obtained a pair of regioisomers, which were demonstrated to be the 1,1′-cyclized compound **13** (yield 67%) and the 1,3′-cyclized compound **14** (yield 9.7%) by NMR and single-crystal X-ray diffractions. Both **13** and **14** are highly π-conjugated heteroarenes with seven fused rings. However, the supposed 3,3′-cyclized regioisomer, **15**, was not found. On the basis of the optimized molecular geometries, the total energy of **15** was calculated to be 0.49 and 0.24 eV higher than those of **13** and **14**, respectively, which can rationalize the higher yield of **13** and the failure for forming **15**.

We also designed route 3 (see Scheme 1) and synthesized the 1-cyclized compound **9** and the 3-cyclized regioisomer **10**, with the yield being 84% and 10%, respectively.

By comparing the three pairs of regioisomers (**9** vs **10**, **11** vs **12**, and **13** vs **14**), we noticed that the 1-cyclized (**9** and **11**) and 1,1′-cyclized (**13**) compounds have higher yields, lower energies, and smaller dipole moments than those of the 3-cyclized (**10** and **12**) and the 1,3′-cyclized (**14**) ones, respectively. We believe that the higher yield of the 1-cyclization can be partly attributed to their lower energies and the formation of intramolecular N−H⋯O hydrogen bonds.

All the new compounds **9**−**14** were fully characterized by ^{1}H NMR, ^{13}C NMR, high-resolution mass spectrometry (HRMS), and X-ray single-crystal diffractions (see Figures 2−4). The spectra/spectrometries and crystallographic data are in the Supporting Information. Generally, the intramolecular N−H⋯O hydrogen bond leads to a downfield shift of the ^{1}H−N NMR signal,[29] and this effect can be conveniently used to identify the regioisomers (**9** vs **10**, **13** vs **14**). As shown in Figure 1, the N−H peak of compound **10** is at 11.57 ppm, while that of its regioisomer **9** is downfield shifted to 12.25 ppm. The 1,1′-cyclized **13** has two same hydrogen bonding N−H protons, and the unique N−H peak was observed at the lower field side of 12.11 ppm. However, the two N−H protons of the asymmetric 1,3′-cyclized **14** are different with the 12.23 and 11.58 ppm peaks corresponding to the N−H⋯O and the N−H with and without intramolecular hydrogen bonding, respectively.

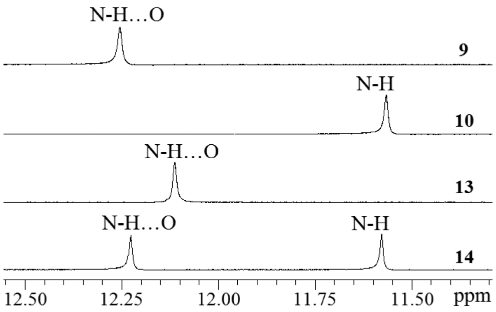

Figure 1. Low-field region of ^{1}H NMR spectra of two pairs of regioisomers (**9** vs **10**, **13** vs **14**) in DMSO-d_6.

2. Structural Characterization. Crystals of compounds **9**−**14** were grown by slow evaporation of their CH_2Cl_2 solutions, and their X-ray structure data are listed in Table 2 and Tables S1−S3. All the molecules of **9**−**14** in their crystals and in the optimized isolated states are planar (Figures 2−4). The 1-cyclized (**9** and **11**), 1,1′-cyclized (**13**), and 1,3′-cyclized (**14**) compounds have intramolecular N−H⋯O hydrogen bonds (listed in Tables S1−S3), which help to form a kind of six-membered ring (see Figures 2 and 3).

As shown in Figure 3, two crescent-shaped molecules of **13** embrace each other by two intermolecular N2−H2⋯O1 hydrogen bonds to pose an X-shaped dimer with a dihedral angle of 50.5°. Molecules are parallelly packed along the *b*-axis direction with the two parallel adjacent molecular dipole moments being in the opposite orientation, giving rise to a type of one-dimensional (1-D) molecular column with alternate $\pi\cdots\pi$ distances of 3.401 and 3.431 Å. Along the *c*-axis direction, neighboring molecular columns are connected by the intermolecular N2−H2⋯O1 hydrogen bonds of the X-shaped dimers. On the basis of the electronic energies of the optimized momomer (E_1) and the optimized dimer (E_2), the energy of the intermolecular N2−H2⋯O1 hydrogen bond was

DOI: 10.1021/acs.joc.8b02939
J. Org. Chem. XXXX, XXX, XXX−XXX

Table 2. Structure Data and Optoelectronic Properties of 1 and 9−14

	1	9	10	11	12	13	14
T (K)		296(2)	294(2)	295(2)	293(2)	295(2)	294(2)
space group		P-1	$P2_1/n$	$C2/c$	P-1	$C2/c$	$P2_12_12_1$
a (Å)		15.5365(7)	7.732(2)	28.3133(6)	7.3885(10)	29.7977(5)	5.6465(8)
b (Å)		15.5527(7)	21.217(6)	7.5509(2)	11.919(2)	7.5553(1)	10.134(2)
c (Å)		25.558(1)	8.849(2)	15.6708(3)	17.597(2)	16.4954(3)	31.872(5)
α (deg)		76.770(1)	90	90	96.437(2)	90	90
β (deg)		76.127(1)	92.940(4)	109.509(1)	90.969(2)	100.342(1)	90
γ (deg)		89.681(1)	90	90	98.162(2)	90	90
V (Å^3)		5828.4(4)	1449.8(6)	3157.9(1)	1523.5(4)	3653.3(1)	1823.7(5)
dipole moment (D)^a		4.223	6.567	5.000	8.088	3.067	5.914
λ_{abs} (nm)^b	400(349.1)	416(383.7)	419(372.3)	425(395.7)	427(382.2)	424(392.4)	433(395.3)
λ_{em} (nm)	412	450^c, 658^d	437	459^c, 678^d	448	445^c, 634^d	454^c, 646^d
τ (ns)	7.0	2.0, 3.2	8.2		5.6	1.3, 1.7	1.5, 1.9
Φ (%)^e	28.8	0.47	31.5	0.29	15.3	1.24	1.9
E_1 (eV)^f	1.34	1.14		1.17		1.09	
E_{HOMO} (eV)^f	−5.67	−5.47		−5.50		−5.42	
energy (hartree)^g	−670.0415	−955.2548	−955.2456	−3528.8082	−3528.7992	−1240.4675	−1240.4588

[a] Calculated values based on optimized geometries. [b] λ_{abs} is the UV absorption maximum in CH_2Cl_2 at the longest wavelength band, and the data in the parentheses are the calculated maximum of the S_0−S_1 transition by TD-DFT/6-311g(d) methods. [c] The K-band emission maximum. [d] The E-band emission maximum in CH_2Cl_2, with $\lambda_{ex} = \lambda_{abs}$. [e] Determined in CH_2Cl_2, using coumarin 307 in MeOH as reference ($\Phi = 0.53$). [f] The first redox potential was measured by cyclic voltammetry with Ag/AgCl reference electrode, see Figure 9. [g] Sum of electronic and zero-point energies, results from DFT calculation at the level of B3LYP/6-311g(d).

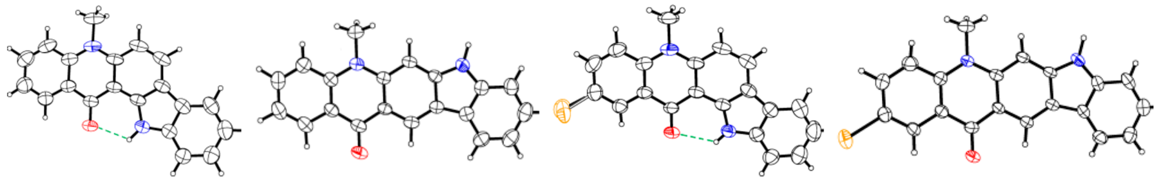
9 **10** **11** **12**

Figure 2. Ortep drawing of the X-ray molecular structures of compounds **9**, **10**, **11**, and **12**.

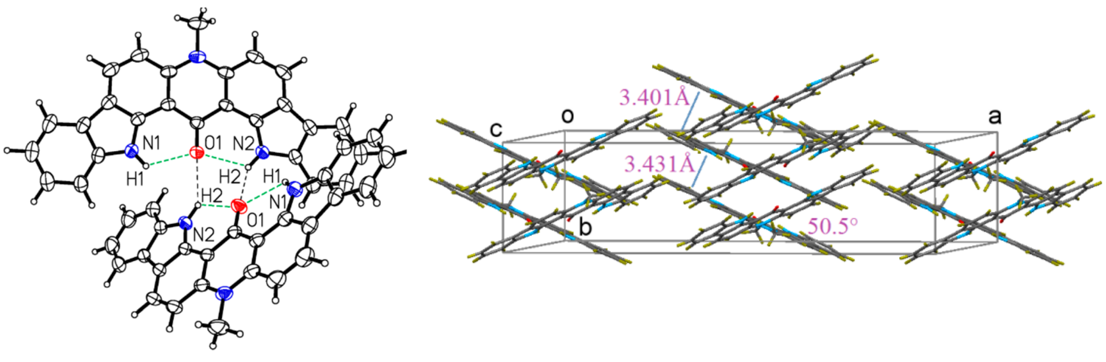

(a) (b)

Figure 3. Crystal structure of compound **13**. (a) The X-shaped dimer connected by the N−H···O hydrogen bonds. (b) The packing diagram, showing the $\pi\cdots\pi$ distances and the dihedral angle of an X-shaped dimer.

calculated to be $(2E_1 - E_2)/2 = 13.0$ kJ/mol (see the Supporting Information for details).

As shown in Figure 4a, the molecule of **14** in the crystal is disordered over two positions. The major position (site occupation factor 53.5%) and the minor position are approximately mirror images of each other. The crystallographic disorder may obscure the molecular structure; fortunately, the correctness of the structure **14** can be supported by the ^{1}H NMR spectra (see Figure 1 and Figure S33). As shown in Figure 4b, four molecules in the unit cell are differently oriented and separately form four 1-D molecular columns along the a-axis direction. All these 1-D molecular columns have a uniform and very short $\pi\cdots\pi$ distance of 3.335 Å, which is favorable for charge transport (vide infra).

3. Photophysical and Electrochemical Properties. As shown in Figure 5a and Table 2, the long-wavelength absorption maximum (λ_{abs}) of compounds **13** (424 nm) and **14** (433 nm) are red-shifted compared to that of **9** (416 nm) and **10** (419 nm), which are in turn red-shifted relative to that of **1** (400 nm), as a result of the π-extension from the three-

DOI: 10.1021/acs.joc.8b02939
J. Org. Chem. XXXX, XXX, XXX−XXX

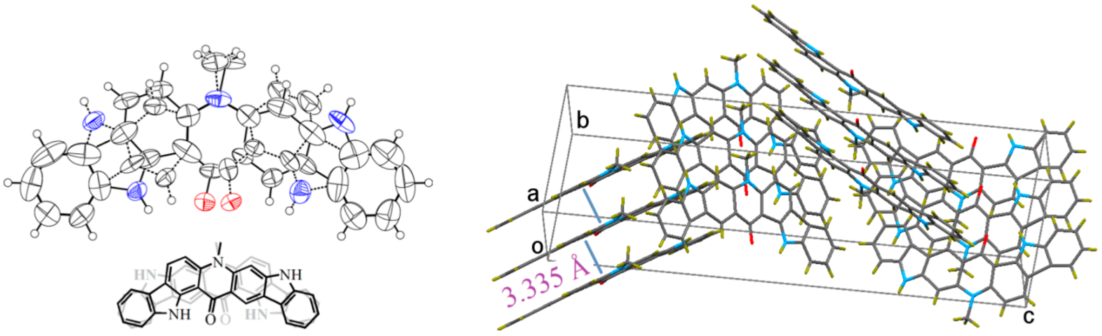

(a) (b)

Figure 4. Crystal structure of compound **14**. (a) The disordered molecule, consisting of the major part (in black and solid line) and the minor part (in gray or dash line). (b) The packing diagram shows the uniform 1-D columnar structure. For clarity, the minor part has been omitted.

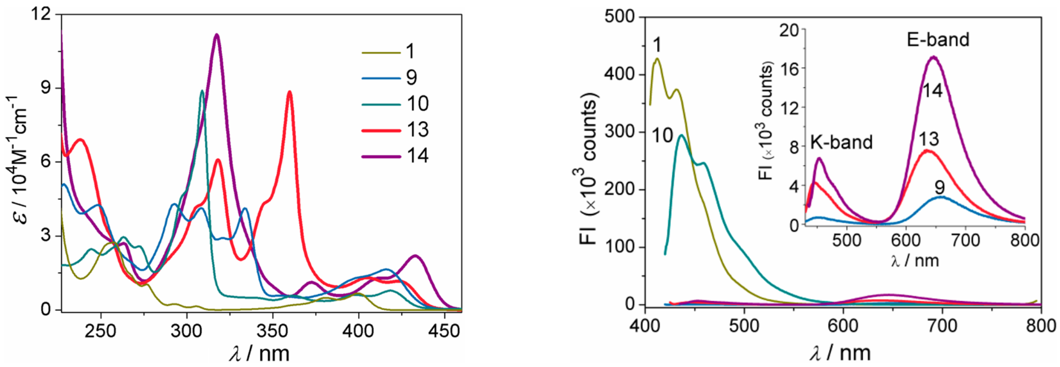

(a) (b)

Figure 5. Absorption spectra (a) and fluorescence spectra (b) for two pairs of regioisomers (**9** vs **10**, **13** vs **14**) and compound **1** in CH_2Cl_2 (c = 20 μM, $\lambda_{ex} = \lambda_{abs}$).

fused-ring to the five-fused-ring and to the seven-fused-ring systems. The TD-DFT-calculated λ_{abs} values (in Table 2) of all these compounds correspond to the HOMO → LUMO transition (Tables S4−S9 and S11).

As shown in Figure 5b, the emission maximum of compound **1** is at 412 nm and the similar emission of 3-cyclized compound **10** is red-shifted to 437 nm. By comparison, the fluorescence spectra of the intramolecular H-bond containing compounds (**9**, **13**, and **14**) consist of two bands. The normal emission band (450 nm for **9**, 445 nm for **13**, and 454 nm for **14**) can be attributed to the K* → K emission of the keto form (K), which is associated with the intramolecular charge-transfer (CT) process (see Figure 6 and Tables S5 and S9−S11). The red-shifted emission band (658 nm for **9**, 634 nm for **13**, and 646 nm for **14**) can be assigned to the E* → E emission of enol form (E). This kind of dual emission can be related to the excited-state intramolecular proton transfer (ESIPT) process.[34−36] Taking compound **13** for example (see Figure 6), upon excitation of the keto form (K) to its charge-transfer state (K*), the K* will emit the K* → K CT band; then, following the K* → E* ESIPT reaction, the E* will emit the red-shifted E* → E band. The K-form of **13** is more stable than the E-form, for the calculated energy of the K-form of **13** is 0.80 eV lower than that of the E-form.

As shown in Figure 7 and Figure S36, the emission intensity ratio (I_E/I_K) of compounds **9**, **13**, and **14** is sensitive to solvent polarity. In nonpolar and aprotic benzene, the fluorescence spectra exhibit prominent E-emission (I_E) and minor K-emission (I_K) with the I_E/I_K ratios of 4.6 (**13**) and 6.1 (**14**).

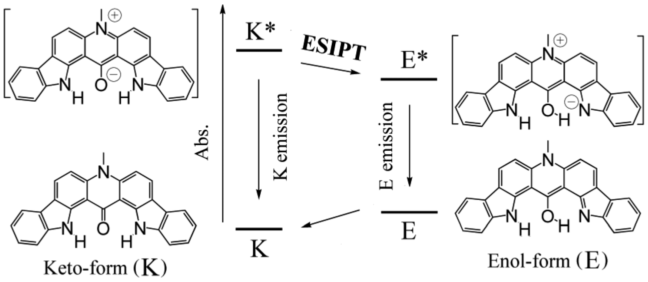

Figure 6. Schematically shown photophysical−photochemical cycle of compound **13**: (1) K → K* intramolecular charge transfer; (2) K*→ E* excited-state intramolecular proton transfer (ESIPT); (3) E* → E intramolecular charge transfer; (4) E→ K ground-state intramolecular reverse proton transfer.

The ratios of I_E/I_K in polar and protic CH_3OH, however, are dramatically decreased to 0.76 (**13**) and 0.56 (**14**). This can be attributed to the intermolecular H-bond characterized solvation in CH_3OH, which is more favorable for the keto form.

The fluorescence spectra of compounds **13** and **14** exhibit a sharp turn-on response to trifluoroacetic acid (TFA). As shown in Figure 8, there appears a new enhancing emission band for both **13** and **14** upon titration with TFA, with a concomitant attenuation of the K-band emission. This new intense band (590 nm for **13** and 583 nm for **14**) is blue-shifted compared to the E-band. Presumably this new band is originated from a kind of trifluoroacetic salt of **13** or **14**.

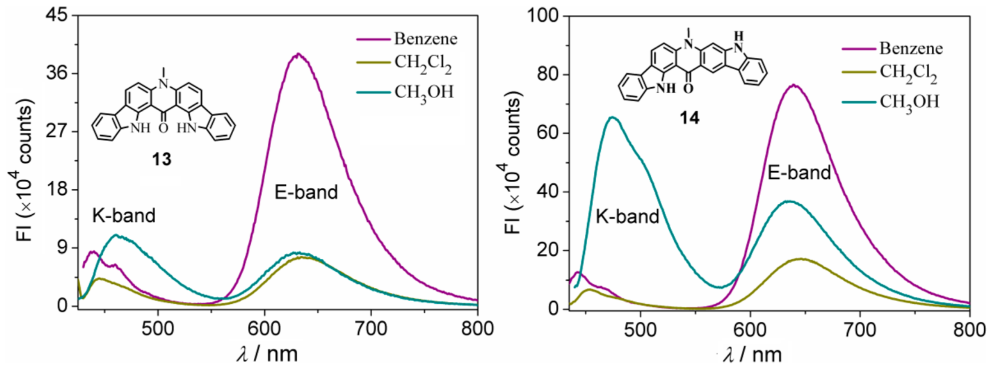

(a) (b)

Figure 7. Fluorescence spectra of **13** (a) and **14** (b) in different solvents (c = 20 μM, λ_{ex} = 425 and 431 nm for **13** and **14** in benzene; λ_{ex} = 423 and 433 nm for **13** and **14** in CH$_2$Cl$_2$; λ_{ex} = 419 and 438 nm for **13** and **14** in CH$_3$OH).

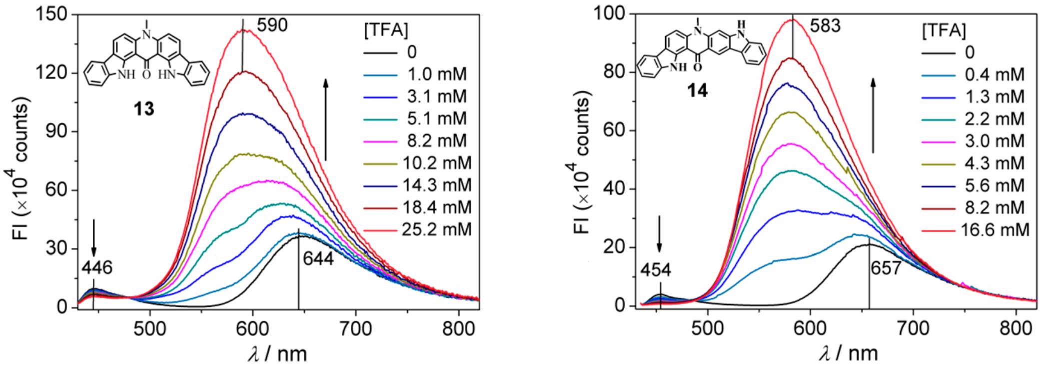

Figure 8. Fluorescence spectra changes of **13** (left, c = 36 μM, λ_{ex} = 423 nm) and **14** (right, c = 21 μM, λ_{ex} = 433 nm) in CH$_2$Cl$_2$ upon titration with TFA.

Crystals of **14**/TFA grown in TFA were obtained, which have different cell parameters to those (in Table 2) of the crystal **14** grown in CH$_2$Cl$_2$. Unfortunately, the **14**/TFA crystal is not good enough for a full X-ray structural determination.

As shown in Figure 9, the first redox pair of the cyclic voltammograms of **9** and **13** is quasi-reversible, while that of the **10** and **14** are irreversible (Figure S41). Ferrocene (Fc) was used as a standard, and its highest occupied molecular orbital (HOMO) energy was taken to be −4.8 eV.[37] The first redox potentials E_1 of **1** and that of the ferrocene were measured to be 1.34 and 0.47 eV, respectively; thus, the HOMO of **1** is −[4.8 + (1.34 − 0.47)] = −5.67 eV. In the same way, the HOMO of **9** and **13** were measured to be −5.47 and −5.42 eV, respectively. These results indicate that with the increase of π-conjugation (from **1** to **9** and to **13**) the electron-donating abilities show the sequence of **1** < **9** < **13**.

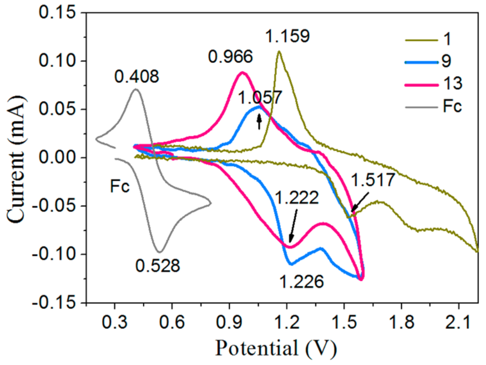

Figure 9. Cyclic voltammograms of **1**, **9**, and **13** in CH$_2$Cl$_2$ (1 mM), scanned at a rate of 50 mV/s with n-Bu$_4$NPF$_6$ (0.1 M) as supporting electrolyte. The Pt wires were used as working and counter electrodes, and Ag/AgCl was used as the reference electrode.

4. Theoretical Survey of the Charge-Transport Properties.

The charge-transport properties of organic crystals depend on many extrinsic parameters (such as temperature and pressure) and materials factors (such as the purity and the perfectness of the crystals).[38] At the microscopic level, the crucial structural variables in the framework of the hopping model (the mobility expression 1) are the reorganization energy λ and the transfer integral t. A hopping hole-transport process

$$M\cdots M^+ \rightarrow M^+\cdots M \tag{2}$$

not only means the transfer of an electron from neutral molecule M to cation M$^+$, but also means the exchange of the geometries between M and M$^+$.

$$M_0^0 + M_+^+ \xrightarrow{\lambda} [M_+^0 + M_0^+] \rightarrow M_+^+ + M_0^0 \tag{3}$$

where the superscript (0 or +) represents the charge of the molecule or its cation (the hole) and the subscript (0 or +) denotes the geometry of the stable molecule or cation.

As illustrated in Figure 10, the λ for the hole transport can be expressed by[39]

$$\lambda = \lambda_1 + \lambda_2 = (E_+^{\ 0} - E_0^{\ 0}) + (E_0^{\ +} - E_+^{\ +}) \tag{4}$$

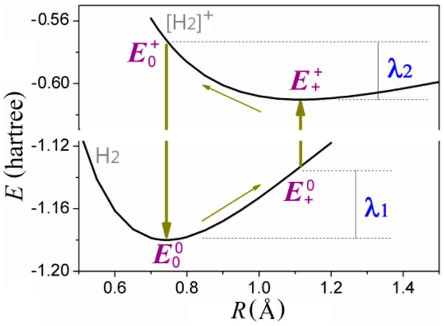

Figure 10. Schematic illustration of a circle of hole transport and the reorganization energy λ; the potential curves here are of the hydrogen molecule H_2 and its cation H_2^+ calculated by DFT/B3LYP/6-311++g(3df,3pd) methods. The shapes of the potential curves can also interpret the fact that for most cases λ_1 and λ_2 are proximately equal.

where λ_1 measures the difference between the energy (E_0^0) of the stable (optimized) molecule and the energy (E_+^0) of the molecule with the stable cation geometry and λ_2 measures the difference between the energy (E_+^+) of the stable (optimized) cation and the energy (E_0^+) of the cation with the stable molecule geometry. All the four terms (E_+^0, E_0^0, E_0^+, and E_+^+) are individually the sum of electronic and zero-point energies. There are no minus frequencies in the calculated results of quinacridone, acridone, **1**, **13**, and **14**. The λ calculation in this work was based on an isolated molecule and its cation without considering the crystalline effect[20] and intermolecular interactions.[40] An exception is for dithiophenetetrathiafulvalene (DT-TTF, see Tables 1 and 3); its λ value was calculated by using the cage model.[20]

The t in eq 1 is a scale of the intermolecular interactions between two neighboring molecules and can be approached by[41]

$$t = \frac{1}{2}(E_{\mathrm{HOMO}} - E_{\mathrm{HOMO}-1}) \tag{5}$$

where E_{HOMO} and $E_{\mathrm{HOMO}-1}$ are the energies of the HOMO and HOMO − 1 of the two-molecule pair, respectively. The t calculation is based on the geometry of the concerned two-molecule pair in the crystal without optimization (see Figure 11).

The λ and t values listed in Table 3 were calculated by DFT/B3LYP/6-311g(d) methods by using the Gaussian 09 program.[42] The d in eq 1 is the distance between the two centroids of the two neighboring molecules in the crystal along the charge-transfer direction.

As shown in Table 3, the C_{2v}- or quasi-C_{2v}-symmetric acridone compounds are characterized by small λ. Compound **1** has 16 π-electrons and a very small λ value (71.5 meV), which is about half the value (λ = 147.5 meV) of the same π-dimensional pyrene (16 π-electrons). To check our calculating methods, the λ value of the well-known organic semiconductor pentacene was also calculated to be 97.9 meV, which is well-consistent with the reported 99.3 meV.[41]

The reorganization energy λ characterizes the charge-transfer barrier, and small λ implies the rigid molecular geometry. The rigidity of the geometry not only means the molecule, but also means the small structural difference between the molecule and its cation. We suppose that one of the necessary conditions for small λ is the same point group of the molecule and its cation. The optimized isolated DT-TTF molecule (see Table 1) has a boat-shaped C_{2v} symmetry (though the crystallized DT-TTF molecule is quasi-D_{2h}[46]); however, the isolated DT-TTF$^+$ cation belongs to planar D_{2h} point group. Thus, the DT-TTF molecule is not very rigid and has a moderate λ value (see Table 3). The large λ value (0.70 eV) of triindole (see entry 3 of Table 1) can be attributed to the inconsistency of the point group in the hole-transport process: the higher symmetric (C_{3h}) triindole molecule degenerates to the lower symmetric (C_s) cation. The similar symmetry degeneration can also be found (see entry 3 of Table 1) for the beautiful coronene ($D_{6h} \rightarrow D_{2h}$) and sulflower ($D_{8h} \rightarrow C_{2h}$). On the other hand, the planar acridone and other planar C_{2v} molecules in Table 1 are invariably C_{2v}-symmetric, from the neutral state to the cation state. These kinds of geometric stable planar molecules may be referred to as rigid-C_{2v}-type molecules.

For the sake of simplicity, only the 1-D hole mobility (μ) along the face-to-face π-columnar direction (see Figure 11) at 300 K has been calculated by eq 1, and the results are listed in Table 3. The calculated μ values of the rigid-C_{2v}-type compounds acridone, **1**, and **13** are significantly larger than that of the semiconductive compound quinacridone. The unexpectedly large μ value of **14** can be attributed to its exceptionally large t value resulting from the very small $\pi\cdots\pi$ distance (3.335 Å). These results indicate that the acridone system may be a promising p-type organic semiconductor material. The μ value of the semiconductive compound DT-TTF along the face-to-edge direction has also been calculated (see Table 3), which can be compared to the experimental results (see Table 3),[4] giving a support to the reliability of the calculating methods.

■ CONCLUSION

In summary, the syntheses, structures, and optoelectronic properties of two series (1-cyclized and 3-cyclized) of new indole-fused acridone derivatives have been reported. The fluorescence spectra of the 1-cyclized compounds exhibit interesting ESIPT. It is well-known that the π-conjugation and

Table 3. Structural Parameters and the Calculated Hole Mobilities (T = 300 K) of Representative Crystals

compds	point group	λ/meV	t/meV	d/Å	μ/cm^2 V^{-1} s^{-1}
quinacridone[a]	C_{2h}	143.4	50.3	3.98	0.85 (0.2)[b]
acridone[a]	C_{2v}	97.7	91.0	4.53	6.84
1[a]	quasi-C_{2v}	71.5	44.1	5.11	3.09
13	quasi-C_{2v}	105.3	51.7[c]	5.35[c]	2.77
14	C_1	108.0	183.7	5.65	37.4
DT-TTF[a]	C_{2v} (D_{2h} for cation)	256.6	100.1	5.81	1.81 (3.6)[b]

[a] The X-ray data for the μ calculation are cited from refs 43 for quinacridone, 44 for acridone, 45 for **1**, and 46 for DT-TTF. [b] The μ values in parentheses are the experimental results cited from refs 31 for quinacridone and 4 for DT-TTF. [c] The average values.

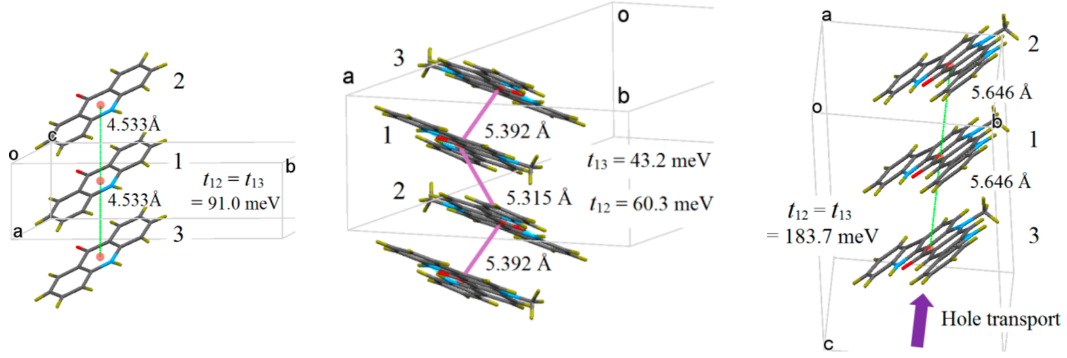

(a) (b) (c)

Figure 11. Charge transport in the 1-D π-columnar structures of compounds (a) acridone, (b) **13**, and (c) **14**. The X-ray data of acridone is from the ref 44.

charge-transfer nature are the two basic structural factors that influence the functions of organic electronic materials. However, the effect of the molecular symmetry on the charge-transport properties of organic semiconductors was rarely concerned. On the basis of the experimental and theoretical studies in this work, we suppose that one of the necessary conditions for low reorganization energy (λ) of crystalline p-type organic semiconductors is the same point group of the molecule and its cation. This work also demonstrated that the planar rigid-C_{2v}-symmetric acridone compounds can have very low charge-transport barrier (small λ) and high mobilities, and therefore they may be a kind of promising hole-transport material.

EXPERIMENTAL SECTION

Syntheses and Chemical Characterization. NMR spectra were recorded on a Bruker AVANCE (300 and 400 MHz) in $CDCl_3$ or DMSO-d_6 with tetramethylsilane (TMS) as an internal reference. The HRMS of compounds **4**−**8** was performed on an electrospray ionization time-of-flight (ESI-TOF) mass spectrometer, and the HRMS of compounds **9**−**14** was performed on a Thermo Fisher Scientific LTQ FTICR-MS instrument with direct analysis in real time (DART) positive ion mode. All the reactions were carried out under N_2 atmosphere using standard Schlenk techniques and heated with an oil bath. Melting points (mp) were measured on a Tektronix XT-4 instrument. UV−vis absorption spectra were recorded on a Shimadzu UV−vis spectrophotometer (UV-2550). Steady-state fluorescence spectra and decay curves were recorded on an Edinburgh FLS920 fluorescence spectrometer equipped with a Xe lamp and a H_2 lamp and a time-correlated single-photon-counting (TCSPC) card. The redox potentials were measured by cyclic voltammetry on a PARSTAT 2273 potentiostat. Compound **1** was synthesized according to literature methods.[47]

*2-Bromo-10-methyl-acridone (**2**).* To a solution of **1** (0.451 g, 2.16 mmol) in 20 mL of DMF was added dropwise a solution of NBS (*N*-bromosuccinimide) (0.460 g, 2.58 mmol) in 10 mL of DMF at 0 °C. The reaction mixture was stirred at 85 °C for 24 h. After cooling to room temperature, the mixture was quenched with water and filtrated. The residue was washed with the mixed solvents of petroleum ether/CH_2Cl_2 (50 mL, 50:1) to give 0.502 g of yellow solid **2** in 81% yield. ^{1}H NMR (300 MHz, $CDCl_3$): δ 8.66 (d, J = 2.4 Hz, 1H), 8.55 (dd, J = 8.0, 1.7 Hz, 1H), 7.80−7.73(m, 2H), 7.54 (d, J = 8.7 Hz, 1H), 7.42 (d, J = 9.0 Hz, 1H), 7.32(t, J = 7.5 Hz, 1H), δ 3.90 (s, 3H). The ^{1}H NMR data of compound **2** are consistent with the reported ^{1}H NMR data of the same compound in ref 48.

*2,7-Dibromo-10-methyl-acridone (**3**).* To a solution of **1** (1.001 g, 4.79 mmol) in 40 mL of DMF was added dropwise a solution of NBS (2.151 g, 12.08 mmol) in 20 mL of DMF at 0 °C. The reaction mixture was stirred at 90 °C for 24 h, and then following the same procedure above for synthesizing **2**, 1.398 g of yellow solid **3** was obtained in 80% yield. ^{1}H NMR (300 MHz, $CDCl_3$): δ 8.65 (d, J = 2.4 Hz, 2H), 7.81 (dd, J = 9.2, 2.6 Hz, 2H), 7.44 (d, J = 9.3 Hz, 2H), 3.89 (s, 3H). The ^{1}H NMR data of compound **3** are consistent with the reported ^{1}H NMR data of the same compound in ref 49.

*2-Bpin-10-methyl-acridone (**4**).* A solution of **2** (0.401 g, 1.40 mmol), bis(pinacolato)diboron (B_2pin_2) (0.519 g, 2.04 mmol), $Pd(dppf)Cl_2(PPh_3)_2$ (0.030 g, 0.041 mmol), and KOAc (0.412 g, 4.21 mmol) in degassed 1,2-dimethoxyethane (DME) (20 mL) was stirred at 80 °C under N_2 for 24 h. After cooling to room temperature, the solvent was removed by rotary evaporation, and the residue was dissolved in CH_2Cl_2. Then, the organic layer was washed with water, dried over anhydrous $MgSO_4$, filtered, and concentrated under reduced pressure. The product was purified by silica gel column chromatography (petroleum ether/ethyl acetate = 8:1) to give 0.451 g of pale yellow solid in 96% yield. ^{1}H NMR (300 MHz, $CDCl_3$): δ 9.04 (d, J = 1.5 Hz, 1H), 8.57 (dd, J = 8.0, 1.7 Hz, 1H), 8.09 (dd, J = 8.7, 1.5 Hz, 1H), 7.72 (t(d,t,d), J = 7.8, 1.8 Hz, 1H), 7.52 (d, J = 8.7 Hz, 1H), 7.48 (d, J = 8.7 Hz, 1H), 7.30 (t, J = 7.4 Hz, 1H), 3.89 (s, 3H), 1.37 (s, 12H). ^{13}C NMR (100 MHz, $CDCl_3$): δ 178.0, 144.5, 142.6, 139.5, 135.7, 133.9, 128.0, 122.9, 121.8, 121.6, 114.9, 113.9, 84.0, 33.8, 25.0. HRMS (ESI) m/z[M + H]$^+$: calcd for $C_{20}H_{23}BNO_3$, 336.1771; found, 336.1768.

*2,7-Bis(Bpin)-10-methyl-acridone (**5**).* A solution of **3** (0.513 g, 1.40 mmol), B_2pin_2 (1.071 g, 4.22 mmol), $Pd(dppf)Cl_2(PPh_3)_2$ (0.030 g, 0.041 mmol), and KOAc (0.827 g, 8.44 mmol) in degassed DME (20 mL) was stirred at 80 °C under N_2 for 24 h, and then following the same procedure above for synthesizing **4**, 0.512 g of pale yellow solid was obtained in 79% yield. ^{1}H NMR (400 MHz, $CDCl_3$): δ 9.05 (s, 2H), 8.11 (d, J = 8.4 Hz, 2H), 7.50 (d, J = 8.8 Hz, 2H), 3.92 (s, 3H), 1.38 (s, 24H). ^{13}C NMR (100 MHz, $CDCl_3$): δ 178.1, 144.5, 139.5, 135.8, 122.4, 114.0, 84.0, 33.9, 25.0. HRMS (ESI) m/z[M + H]$^+$: calcd for $C_{26}H_{34}B_2NO_5$, 462.2623; found, 462.2617.

*2-(2-Nitrophenyl)-10-methyl-acridone (**6**).* To a solution of **4** (0.450 g, 1.34 mmol), 2-nitroiodobenzene (0.401 g, 1.61 mmol), and K_2CO_3 (0.556 g, 4.03 mmol) in 24 mL of degassed solvents of DME/H_2O (5:1) was added $Pd(PPh_3)_4$ (0.050 g, 0.043 mmol). Then, the mixture was heated to 100 °C under N_2 for 24 h. After the reaction mixture was cooled to rt, the DME was removed by rotary evaporation. The residue was dissolved in CH_2Cl_2, and then the organic layer was washed with water, dried over anhydrous $MgSO_4$, filtered, and concentrated under reduced pressure. The product was purified by silica gel column chromatography (petroleum ether/CH_2Cl_2 = 1:3) to give 0.333 g of orange powder in 75% yield. Mp 237−238 °C. ^{1}H NMR (400 MHz, $CDCl_3$): δ 8.603 (d, J = 10.4 Hz, 1H), 8.599 (d, J = 10.0 Hz, 1H), 7.95 (dd, J = 8.0, 1.2 Hz, 1H), 7.78 (t(d,t,d), J = 7.8, 1.6 Hz, 1H), 7.70−7.64 (m, 2H), 7.61−7.57 (m, 3H), 7.53 (t(d,s,d), J = 7.8, 1.2 Hz, 1H), 7.35 (t, J = 7.6 Hz, 1H), 3.96 (s, 3H). ^{13}C NMR (100 MHz, $CDCl_3$): δ 177.8, 149.0, 142.5, 142.3, 135.4, 134.1, 133.4, 132.7, 132.5, 130.6, 128.4, 127.9, 127.2, 124.5, 122.7, 122.5, 121.7, 115.3, 114.9, 33.8. HRMS (ESI) $m/z[M + H]^+$: calcd for $C_{20}H_{15}N_2O_3$, 331.1083; found, 331.1078.

*2-(2-Nitrophenyl)-7-bromo-10-methyl-acridone (**7**).* To a solution of **3** (0.153 g, 0.417 mmol), 2-nitrophenylboronic acid (0.300 g, 1.80 mmol), and K_2CO_3 (0.350 g, 2.53 mmol) in 12 mL of degassed solvents of DME/H_2O (5:1) was added $Pd(PPh_3)_4$ (0.019 g, 0.016 mmol). Then, the mixture was heated to 100 °C under N_2 for 48 h. After cooling to rt, 60 mL of CH_2Cl_2 was added to the reaction mixture with stirring to extract the product to the liquid phase. Then, after the insolvables were filtered out, the organic liquid phase was washed with a large amount of water to remove DME and residual inorganic salts in solution. The resultant crude product was purified by silica gel column chromatography (CH_2Cl_2) to obtain 0.055 g of crystalline orange powder of **7** in 32% yield. ^1H NMR (400 MHz, $CDCl_3$): δ 8.70 (d, J = 2.4 Hz, 1H), 8.58 (d, J = 2.0 Hz, 1H), 7.96 (dd, J = 8.0, 1.2 Hz, 1H), 7.83 (dd, J = 9.2, 2.4 Hz, 1H), 7.70−7.65 (m, 1H), 7.67 (d, J = 8.8 Hz, 1H), 7.59 (d, J = 8.4 Hz, 1H), 7.57 (dd, J = 7.6, 1.6 Hz, 1H), 7.56−7.52 (m, 1H), 7.48 (d, J = 9.2 Hz, 1H), 3.95 (s, 3H). ^{13}C NMR (100 MHz, $CDCl_3$): δ 149.0, 136.8, 135.2, 133.7, 132.7, 132.4, 131.0, 130.3, 128.5, 127.3, 124.5, 124.0, 123.2, 122.6, 116.9, 115.3, 115.1, 34.0. HRMS (ESI) $m/z[M + H]^+$: calcd for $C_{20}H_{14}BrN_2O_3$, 409.0188; found, 409.0186.

*2,7-Bis(2-nitrophenyl)-10-methyl-acridone (**8**).* To a solution of **5** (0.813 g, 1.76 mmol), 2-nitroiodobenzene (1.351 g, 5.43 mmol), and K_2CO_3 (1.458 g, 10.57 mmol) in 36 mL of degassed DME/H_2O (5:1) was added $Pd(PPh_3)_4$ (0.100 g, 0.087 mmol). The mixture was heated to 100 °C under N_2 for 24 h. Then, the same subsequent treatment of synthesizing compound **6** was carried out to obtain crude product, which was purified by silica gel column chromatography (petroleum ether/CH_2Cl_2 = 1:2) to give 0.556 g of yellow solid in 70% yield. Mp 253−254 °C. ^1H NMR (400 MHz, $CDCl_3$): δ 8.62 (s, 2H), 7.96 (d, J = 8.0 Hz, 2H), 7.69−7.67 (m, 4H), 7.63 (d, J = 9.2 Hz, 2H), 7.60 (d, J = 7.6 Hz, 2H), 7.54 (t, J = 7.4 Hz, 2H), 4.01 (s, 3H). ^{13}C NMR (100 MHz, $CDCl_3$): δ 177.6, 149.0, 142.3, 135.3, 133.6, 132.7, 132.5, 131.0, 128.5, 127.3, 124.5, 122.7, 115.4, 34.0. HRMS (ESI) $m/z[M + H]^+$: calcd for $C_{26}H_{18}N_3O_6$, 452.1246; found, 452.1250.

*10-Methyl-indolo[2,3-a]acridone (**9**) and 10-Methyl-indolo[3,2-b]acridone (**10**).* To a solution of **6** (0.425 g, 1.29 mmol) in 6 mL of degassed 1,2-dichlorobenzene (o-DCB) was added PPh_3 (1.013 g, 3.87 mmol). Then, the mixture was heated to 180 °C under N_2 for 24 h. After the reaction mixture was cooled to rt, it was directly mixed with excess amount of silica gel powder, and then purified by silica gel column chromatography. The first main component was eluted out by an eluent of petroleum ether/CH_2Cl_2 = 1:2, obtaining 0.322 g of **9** in 84% yield. The second component was eluted out by pure CH_2Cl_2, obtaining 0.040 g of **10** in 10% yield.

*Characterization Data of **9**.* Mp 284−285 °C. ^1H NMR (300 MHz, $CDCl_3$): δ 11.51 (s, 1H), 8.65 (dd, J = 8.1, 1.5 Hz, 1H), 8.35 (d, J = 9.0 Hz, 1H), 8.08 (d, J = 7.8 Hz, 1H), 7.76 (t(d,t,d), J = 7.8, 1.5 Hz, 1H), 7.63 (d, J = 8.1 Hz, 1H), 7.61 (d, J = 8.7 Hz, 1H), 7.46 (td, J = 7.7, 1.2 Hz, 1H), 7.37 (td, J = 7.4, 0.75 Hz, 1H), 7.31 (t, J = 8.3 Hz, 1H), 7.30 (d, J = 8.7 Hz, 1H), 4.01 (s, 3H). ^{13}C NMR (100 MHz, $CDCl_3$): δ 178.9, 142.1, 141.6, 139.2, 139.1, 133.3, 126.9, 126.9, 124.9, 122.9, 122.2, 121.4, 120.1, 119.4, 116.1, 115.0, 111.5, 108.1, 105.5, 34.6 ppm. MS (DART) $m/z[M + H]^+$: 299.1. HRMS (DART) $m/z[M + H]^+$: calcd for $C_{20}H_{15}ON_2$, 299.1179; found, 299.1176.

*Characterization Data of **10**.* Mp > 300 °C. ^1H NMR (300 MHz, DMSO-d_6): δ 11.57 (s, 1H), 9.11 (s, 1H), 8.40 (dd, J = 8.0, 1.1 Hz, 1H), 8.28 (d, J = 7.8 Hz, 1H), 7.87−7.78 (m, 2H), 7.61 (s, 1H), 7.52 (d, J = 8.1 Hz, 1H), 7.44 (td, J = 7.7, 1.2 Hz, 1H), 7.31 (t(d,t,d), J = 7.1, 1.5 Hz, 1H), 7.23 (t(d,s,d), J = 7.4, 1.2 Hz, 1H), 4.01 (s, 3H). ^{13}C NMR (100 MHz, DMSO-d_6): δ 177.2, 145.2, 143.0, 142.2, 142.0, 134.0, 127.1, 126.9, 123.0, 121.4, 121.1, 120.9, 120.1, 119.8, 119.6, 116.5, 116.1, 111.4, 95.0, 34.6 ppm. MS (DART) $m/z[M + H]^+$: 299.1. HRMS (DART) $m/z[M + H]^+$: calcd for $C_{20}H_{15}ON_2$, 299.1179; found, 299.1177.

*7-Bromo-10-methyl-indolo[2,3-a]acridone (**11**) and 7-Bromo-10-methyl-indolo[3,2-b]acridone (**12**).* To a solution of **7** (0.180 g, 0.440 mmol) in 5 mL of degassed o-DCB was added PPh_3 (1.001 g, 3.82 mmol). Then, the mixture was heated to 180 °C under N_2 for 36 h. After the reaction mixture was cooled to rt, it was directly mixed with excess amount of silica gel powder, and then purified by silica gel column chromatography. The first main component was eluted out by an eluent of petroleum ether/CH_2Cl_2 = 1:2, obtaining 0.141 g of **11** in 85% yield. The second component was eluted out by an eluent of petroleum ether/CH_2Cl_2 = 1:5, obtaining 0.023 g of **12** in 14% yield.

*Characterization Data of **11**.* Mp > 300 °C. ^1H NMR (400 MHz, $CDCl_3$): δ 11.46 (s, 1H), 8.76 (d, J = 2.4 Hz, 1H), 8.42 (d, J = 8.8 Hz, 1H), 8.11 (d, J = 7.6 Hz, 1H), 7.83 (dd, J = 9.2, 2.4 Hz, 1H), 7.65 (d, J = 8.4 Hz, 1H), 7.54 (d, J = 9.2 Hz, 1H), 7.48 (t(d,s,d), J = 7.7, 1.0 Hz, 1H), 7.34 (d, J = 8.8 Hz, 1H), 7.34 (t, J = 7.2 Hz, 1H), 4.04 (s, 3H). ^{13}C NMR (100 MHz, $CDCl_3$): δ 136.1, 129.4, 127.3, 125.2, 120.3, 119.5, 117.1, 111.6, 105.5, 34.8, 29.7 ppm (because of the poor solubility the ^{13}C NMR spectra is incomplete.). MS (DART) $m/z[M + H]^+$: 379.0. HRMS (DART) $m/z[M + H]^+$: calcd for $C_{20}H_{14}ON_2Br$, 377.0284; found, 377.0281

*Characterization Data of **12**.* Mp > 300 °C. ^1H NMR (300 MHz, DMSO-d_6): δ 11.60 (s, 1H), 9.10 (s, 1H), 8.43 (d, J = 2.4 Hz, 1H), 8.28 (d, J = 7.8 Hz, 1H), 7.91 (dd, J = 9.3, 2.4 Hz, 1H), 7.83 (d, J = 9.3 Hz, 1H), 7.61 (s, 1H), 7.52 (d, J = 8.1 Hz, 1H), 7.45 (td, J = 7.5, 1.2 Hz, 1H), 7.24 (t(d,s,d), J = 7.4, 1.1 Hz, 1H), 3.98 (s, 3H). ^{13}C NMR (100 MHz, DMSO-d_6): δ 176.0, 145.3, 142.0, 142.0, 141.8, 136.2, 128.9, 127.1, 122.9, 122.7, 121.2, 120.2, 120.2, 119.6, 119.0, 116.3, 113.1, 111.5, 95.2, 34.8 ppm. MS (DART) $m/z[M + H]^+$: 379.0. HRMS (DART) $m/z[M + H]^+$: calcd for $C_{20}H_{14}ON_2Br$, 377.0284; found, 377.0280.

*10-Methyl-indolo[2,3-a]-indolo[2,3-a′]acridone (**13**) and 10-Methyl-indolo[2,3-a]-indolo[3,2-b′]acridone (**14**).* To a solution of **8** (0.628 g, 1.391 mmol) in 10 mL of degassed o-DCB was added PPh_3 (2.501 g, 9.54 mmol). Then, the mixture was heated to 180 °C under N_2 for 36 h. After the reaction mixture was cooled to rt, it was directly mixed with excess amount of silica gel powder, and then purified by silica gel column chromatography. The first main component was eluted out by an eluent of petroleum ether/CH_2Cl_2 = 1:2, obtaining 0.362 g of **13** in 67% yield. The second component was eluted out by an eluent of petroleum ether/CH_2Cl_2 = 1:4, obtaining 0.052 g of **14** in 9.7% yield.

*Characterization Data of **13**.* Mp > 300 °C. ^1H NMR (400 MHz, $CDCl_3$): δ 11.61 (s, 2H), 8.44 (d, J = 9.2 Hz, 2H), 8.15 (d, J = 8.0 Hz, 2H), 7.68 (d, J = 8.0 Hz, 2H), 7.49 (t, J = 8.2 Hz, 2H), 7.46 (d, J = 9.2 Hz, 2H), 7.35 (t, J = 7.6 Hz, 2H), 4.19 (s, 3H). ^{13}C NMR (100 MHz, $CDCl_3$): δ 126.5, 125.0, 120.1, 119.5, 111.5, 106.0, 29.7 ppm (because of the poor solubility the ^{13}C NMR spectra is incomplete). MS (DART) $m/z[M + H]^+$: 388.1. HRMS (DART) $m/z[M + H]^+$: calcd for $C_{26}H_{18}ON_3$, 388.1444; found, 388.1439.

*Characterization Data of **14**.* Mp > 300 °C. ^1H NMR (400 MHz, DMSO-d_6): δ 12.23 (s, 1H), 11.58 (s, 1H), 9.22 (s, 1H), 8.55 (d, J = 8.8 Hz, 1H), 8.31 (d, J = 7.6 Hz, 1H), 8.18 (d, J = 7.6 Hz, 1H), 7.88 (d, J = 8.0 Hz, 1H), 7.72 (s, 1H), 7.62 (d, J = 9.2 Hz, 1H), 7.55 (d, J = 7.6 Hz, 1H), 7.47 (t, J = 7.6 Hz, 1H), 7.40 (t, J = 7.6 Hz, 1H), 7.26 (t, J = 7.0 Hz, 1H), 7.25 (t, J = 7.4 Hz, 1H), 4.14 (s, 3H). ^{13}C NMR (100 MHz, DMSO-d_6): δ 178.0, 144.8, 142.4, 142.0, 141.7, 139.9, 138.6, 127.0, 126.9, 124.8, 123.0, 122.2, 121.1, 120.0, 119.8, 119.6, 118.7, 117.0, 115.7, 112.9, 111.4, 107.0, 106.9, 95.3, 35.7 ppm. MS (DART) $m/z[M + H]^+$: 388.1. HRMS (DART) $m/z[M + H]^+$: calcd for $C_{26}H_{18}ON_3$, 388.1444; found, 388.1441.

Calculation and X-ray Structure Determination. All the quantum chemistry calculations were carried out by using DFT or TD-DFT methods by the Gaussian 09 program.[42] All the single-crystal X-ray determinations were carried out by a Bruker APEXII CCD diffractometer (Mo $K\alpha$ radiation). The structures were solved by direct methods using SHELXL-2014 programs.[50] The atomic ellipsoids in Figures 2−4 were drawn at the 50% probability level. All hydrogen atoms of crystals **9**−**13** were located in the difference Fourier maps and refined freely, except the hydrogen atoms of the methyl group which were geometrically added and refined using a riding model. The hydrogen atoms of crystals **14** were geometrically added because of the heavy crystallographic disorder. All the **9**−**14**

structure data were sent to the Web of International Union of Crystallography for checking, and the checkCIF reports concluded no A, B level of alerts.

■ ASSOCIATED CONTENT

Supporting Information

The Supporting Information is available free of charge on the ACS Publications website at DOI: 10.1021/acs.joc.8b02939.

> ^{1}H NMR of compounds **2** and **3**, ^{1}H NMR, ^{13}C NMR, and HRMS of compounds **4–14**, X-ray crystallographic structure data of compounds **9–14**, TD-DFT calculated spectral transition properties of **1** and **9–14**, fluorescence spectra of **9** and **10** in various solvents, fluorescence decay curves of **1**, **9**, **10**, **12**, **13**, and **14**, fluorescence spectra of **9**, **13**, and **14** in films, fluorescence spectra of **14** upon titration of CH_3COOH, cyclic voltammograms of compounds **10**, **11**, **12**, and **14**, energies and Cartesian coordinates table for compounds **1** and **9–14**, the calculation for the intermolecular N2–H2···O1 hydrogen bond of **13**, and computational details for reorganization energies (PDF)
>
> X-ray crystal details for **9** (CIF)
>
> X-ray crystal details for **10** (CIF)
>
> X-ray crystal details for **11** (CIF)
>
> X-ray crystal details for **12** (CIF)
>
> X-ray crystal details for **13** (CIF)
>
> X-ray crystal details for **14** (CIF)

■ AUTHOR INFORMATION

Corresponding Author

*E-mail: fangqi@sdu.edu.cn.

ORCID

Qi Fang: 0000-0001-8024-2875

Notes

The authors declare no competing financial interest.

■ ACKNOWLEDGMENTS

This work was supported by the National Natural Science Foundation of China (Grant Nos. 21472116 and 21871165) and the State Key Laboratory of Crystal Materials. The authors thank Professor Zhi-qiang Liu for the discussions about the synthesis methods, Professor Hong Lei for the mobility calculation, and Professor Lei Ji and Dr. Ye Fang for assistance in editing the text of this manuscript.

■ REFERENCES

(1) Tsumura, A.; Koezuka, H.; Ando, T. Macromolecular electronic device: Field-effect transistor with a polythiophene thin film. *Appl. Phys. Lett.* **1986**, *49*, 1210–1212.

(2) Wang, C.; Dong, H.; Hu, W.; Liu, Y.; Zhu, D. Semiconducting π-Conjugated Systems in Field-Effect Transistors: A Material Odyssey of Organic Electronics. *Chem. Rev.* **2012**, *112*, 2208–2267.

(3) Mei, J.; Diao, Y.; Appleton, A. L.; Fang, L.; Bao, Z. Integrated Materials Design of Organic Semiconductors for Field-Effect Transistors. *J. Am. Chem. Soc.* **2013**, *135*, 6724–6746.

(4) Mas-Torrent, M.; Rovira, C. Role of Molecular Order and Solid-State Structure in Organic Field-Effect Transistors. *Chem. Rev.* **2011**, *111*, 4833–4856.

(5) Takimiya, K.; Shinamura, S.; Osaka, I.; Miyazaki, E. Thienoacene-Based Organic Semiconductors. *Adv. Mater.* **2011**, *23*, 4347–4370.

(6) Jurchescu, O. D.; Popinciuc, M.; van Wees, B. J.; Palstra, T. T. M. Interface-Controlled, High-Mobility Organic Transistors. *Adv. Mater.* **2007**, *19*, 688–692.

(7) Sundar, V. C.; Zaumseil, J.; Podzorov, V.; Menard, E.; Willett, R. L.; Someya, T.; Gershenson, M. E.; Rogers, J. A. Elastomeric Transistor Stamps: Reversible Probing of Charge Transport in Organic Crystals. *Science* **2004**, *303*, 1644–1646.

(8) Jiang, W.; Zhou, Y.; Geng, H.; Jiang, S.; Yan, S.; Hu, W.; Wang, Z.; Shuai, Z.; Pei, J. Solution-Processed, High-Performance Nanoribbon Transistors Based on Dithioperylene. *J. Am. Chem. Soc.* **2011**, *133*, 1–3.

(9) Takahashi, Y.; Hasegawa, T.; Horiuchi, S.; Kumai, R.; Tokura, Y.; Saito, G. High Mobility Organic Field-Effect Transistor Based on Hexamethylenetetrathiafulvalene with Organic Metal Electrodes. *Chem. Mater.* **2007**, *19*, 6382–6384.

(10) Xu, X.; Yao, Y.; Shan, B.; Gu, X.; Liu, D.; Liu, J.; Xu, J.; Zhao, N.; Hu, W.; Miao, Q. Electron Mobility Exceeding 10 $cm^2 V^{-1} s^{-1}$ and Band-Like Charge Transport in Solution-Processed n-Channel Organic Thin-Film Transistors. *Adv. Mater.* **2016**, *28*, 5276–5283.

(11) Briseno, A. L.; Miao, Q.; Ling, M.-M.; Reese, C.; Meng, H.; Bao, Z.; Wudl, F. Hexathiapentacene: Structure, Molecular Packing, and Thin-Film Transistors. *J. Am. Chem. Soc.* **2006**, *128*, 15576–15577.

(12) Zhang, C.; Zang, Y.; Gann, E.; McNeill, C. R.; Zhu, X.; Di, C.; Zhu, D. Two-Dimensional π-Expanded Quinoidal Terthiophenes Terminated with Dicyanomethylenes as n-Type Semiconductors for High-Performance Organic Thin-Film Transistors. *J. Am. Chem. Soc.* **2014**, *136*, 16176–16184.

(13) Gsänger, M.; Kirchner, E.; Stolte, M.; Burschka, C.; Stepanenko, V.; Pflaum, J.; Würthner, F. High-Performance Organic Thin-Film Transistors of J-Stacked Squaraine Dyes. *J. Am. Chem. Soc.* **2014**, *136*, 2351–2362.

(14) Usta, H.; Risko, C.; Wang, Z.; Huang, H.; Deliomeroglu, M. K.; Zhukhovitskiy, A.; Facchetti, A.; Marks, T. J. Design, Synthesis, and Characterization of Ladder-Type Molecules and Polymers. Air-Stable, Solution-Processable n-Channel and Ambipolar Semiconductors for Thin-Film Transistors via Experiment and Theory. *J. Am. Chem. Soc.* **2009**, *131*, 5586–5608.

(15) Dou, J.-H.; Zheng, Y.-Q.; Yao, Z.-F.; Yu, Z.-A.; Lei, T.; Shen, X.; Luo, X.-Y.; Sun, J.; Zhang, S.-D.; Ding, Y.-F.; Han, G.; Yi, Y.; Wang, J.-Y.; Pei, J. Fine-Tuning of Crystal Packing and Charge Transport Properties of BDOPV Derivatives through Fluorine Substitution. *J. Am. Chem. Soc.* **2015**, *137*, 15947–15956.

(16) Jiang, W.; Li, Y.; Wang, Z. Tailor-Made Rylene Arrays for High Performance n-Channel Semiconductors. *Acc. Chem. Res.* **2014**, *47*, 3135–3147.

(17) Xiong, Y.; Qiao, X.; Wu, H.; Huang, Q.; Wu, Q.; Li, J.; Gao, X.; Li, H. Syntheses and Properties of Nine-Ring-Fused Linear Thienoacenes. *J. Org. Chem.* **2014**, *79*, 1138–1144.

(18) Marcus, R. A. Electron transfer reactions in chemistry. Theory and experiment. *Rev. Mod. Phys.* **1993**, *65*, 599–610.

(19) Balzani, V.; Juris, A.; Venturi, M.; Campagna, S.; Serroni, S. Luminescent and Redox-Active Polynuclear Transition Metal Complexes. *Chem. Rev.* **1996**, *96*, 759–833.

(20) Fang, Q.; Chen, H.; Lei, H.; Xue, G.; Chen, X. Full-capped 12-S-atom TTP derivatives (BV-TTP, BE-TTP, EM-TTP and EV-TTP): syntheses, structures and charge transport properties. *CrystEngComm* **2015**, *17*, 787–796.

(21) Li, R.; Jiang, L.; Meng, Q.; Gao, J.; Li, H.; Tang, Q.; He, M.; Hu, W.; Liu, Y.; Zhu, D. Micrometer-Sized Organic Single Crystals, Anisotropic Transport, and Field-Effect Transistors of a Fused-Ring Thienoacene. *Adv. Mater.* **2009**, *21*, 4492–4495.

(22) Okamoto, T.; Kudoh, K.; Wakamiya, A.; Yamaguchi, S. General Synthesis of Thiophene and Selenophene-Based Heteroacenes. *Org. Lett.* **2005**, *7*, 5301–5304.

(23) Okamoto, T.; Mitsui, C.; Yamagishi, M.; Nakahara, K.; Soeda, J.; Hirose, Y.; Miwa, K.; Sato, H.; Yamano, A.; Matsushita, T.; Uemura, T.; Takeya, J. V-Shaped Organic Semiconductors With

Solution Processability, High Mobility, and High Thermal Durability. *Adv. Mater.* **2013**, *25*, 6392−6397.

(24) Rieger, R.; Beckmann, D.; Mavrinskiy, A.; Kastler, M.; Müllen, K. Backbone Curvature in Polythiophenes. *Chem. Mater.* **2010**, *22*, 5314−5318.

(25) Laquindanum, J. G.; Katz, H. E.; Lovinger, A. J. Synthesis, Morphology, and Field-Effect Mobility of Anthradithiophenes. *J. Am. Chem. Soc.* **1998**, *120*, 664−672.

(26) Mamada, M.; Katagiri, H.; Mizukami, M.; Honda, K.; Minamiki, T.; Teraoka, R.; Uemura, T.; Tokito, S. *syn-/anti-*Anthradithiophene Derivative Isomer Effects on Semiconducting Properties. *ACS Appl. Mater. Interfaces* **2013**, *5*, 9670−9677.

(27) Niimi, K.; Shinamura, S.; Osaka, I.; Miyazaki, E.; Takimiya, K. Dianthra[2,3-*b*:2′,3′-*f*]thieno[3,2-*b*]thiophene (DATT): Synthesis, Characterization, and FET Characteristics of New π-Extended Heteroarene with Eight Fused Aromatic Rings. *J. Am. Chem. Soc.* **2011**, *133*, 8732−8739.

(28) Yamamoto, K.; Higashibayashi, S. Synthesis of Three-Dimensional Butterfly Slit-Cyclobisazaanthracenes and Hydrazinobisanthenes through One-Step Cyclodimerization and Their Properties. *Chem. - Eur. J.* **2016**, *22*, 663−671.

(29) Mamada, M.; Inada, K.; Komino, T.; Potscavage, W. J., Jr.; Nakanotani, H.; Adachi, C. Highly Efficient Thermally Activated Delayed Fluorescence from an Excited-State Intramolecular Proton Transfer System. *ACS Cent. Sci.* **2017**, *3*, 769−777.

(30) Chen, W.; Tian, K.; Song, X.; Zhang, Z.; Ye, K.; Yu, G.; Wang, Y. Large π-Conjugated Quinacridone Derivatives: Syntheses, Characterizations, Emission, and Charge Transport Properties. *Org. Lett.* **2015**, *17*, 6146−6149.

(31) Głowacki, E. D.; Irimia-Vladu, M.; Kaltenbrunner, M.; Gąsiorowski, J.; White, M. S.; Monkowius, U.; Romanazzi, G.; Suranna, G. P.; Mastrorilli, P.; Sekitani, T.; Bauer, S.; Someya, T.; Torsi, L.; Sariciftci, N. S. Hydrogen-Bonded Semiconducting Pigments for Air-Stable Field-Effect Transistors. *Adv. Mater.* **2013**, *25*, 1563−1569.

(32) Chen, D.-M.; Qin, Q.; Sun, Z.-B.; Peng, Q.; Zhao, C.-H. Synthesis and properties of B,N-bridged *p*-terphenyls. *Chem. Commun.* **2014**, *50*, 782−784.

(33) Kim, H.; Kim, B.; Kim, Y.; Kim, C.; Shin, C.; Lee, S.; Yu, E.; Choi, B.; Hwang, K. Condensed cyclic compound and organic light-emitting device. European Patent EP2894157A1, July 15, 2015.

(34) Kwon, J. E.; Park, S. Y. Advanced Organic Optoelectronic Materials: Harnessing Excited-State Intramolecular Proton Transfer (ESIPT) Process. *Adv. Mater.* **2011**, *23*, 3615−3642.

(35) Demchenko, A. P.; Tang, K.-C.; Chou, P.-T. Excited-state proton coupled charge transfer modulated by molecular structure and media polarization. *Chem. Soc. Rev.* **2013**, *42*, 1379−1408.

(36) Zhang, Z.; Chen, Y.-A.; Hung, W.-Y.; Tang, W.-F.; Hsu, Y.-H.; Chen, C.-L.; Meng, F.-Y.; Chou, P.-T. Control of the Reversibility of Excited-State Intramolecular Proton Transfer (ESIPT) Reaction: Host-Polarity Tuning White Organic Light Emitting Diode on a New Thiazolo[5,4-*d*]thiazole ESIPT System. *Chem. Mater.* **2016**, *28*, 8815−8824.

(37) Thelakkat, M.; Schmidt, H.-W. Synthesis and Properties of Novel Derivatives of 1,3,5-Tris(diarylamino)benzenes for Electroluminescent Devices. *Adv. Mater.* **1998**, *10*, 219−223.

(38) Schweicher, G.; Olivier, Y.; Lemaur, V.; Geerts, Y. H. What Currently Limits Charge Carrier Mobility in Crystals of Molecular Semiconductors? *Isr. J. Chem.* **2014**, *54*, 595−620.

(39) Berlin, Y. A.; Hutchison, G. R.; Rempala, P.; Ratner, M. A.; Michl, J. Charge Hopping in Molecular Wires as a Sequence of Electron-Transfer Reactions. *J. Phys. Chem. A* **2003**, *107*, 3970−3980.

(40) Vaissier, V.; Frost, J. M.; Barnes, P. R. F.; Nelson, J. Influence of Intermolecular Interactions on the Reorganization Energy of Charge Transfer between Surface-Attached Dye Molecules. *J. Phys. Chem. C* **2015**, *119*, 24337−24341.

(41) Deng, W.-Q.; Goddard, W. A., III Predictions of Hole Mobilities in Oligoacene Organic Semiconductors from Quantum Mechanical Calculations. *J. Phys. Chem. B* **2004**, *108*, 8614−8621.

(42) Frisch, M. J.; Trucks, G. W.; Schlegel, H. B.; Scuseria, G. E.; Robb, M. A.; Cheeseman, J. R.; Scalmani, G.; Barone, V.; Mennucci, B.; Petersson, G. A.; Nakatsuji, H.; Caricato, M.; Li, X.; Hratchian, H. P.; Izmaylov, A. F.; Bloino, J.; Zheng, G.; Sonnenberg, J. L.; Hada, M.; Ehara, M.; Toyota, K.; Fukuda, R.; Hasegawa, J.; Ishida, M.; Nakajima, T.; Honda, Y.; Kitao, O.; Nakai, H.; Vreven, T.; Montgomery, J. A.; Peralta, J. E., Jr.; Ogliaro, F.; Bearpark, M.; Heyd, J. J.; Brothers, E.; Kudin, K. N.; Staroverov, V. N.; Kobayashi, R.; Normand, J.; Raghavachari, K.; Rendell, A.; Burant, J. C.; Iyengar, S. S.; Tomasi, J.; Cossi, M.; Rega, N.; Millam, J. M.; Klene, M.; Knox, J. E.; Cross, J. B.; Bakken, V.; Adamo, C.; Jaramillo, J.; Gomperts, R.; Stratmann, R. E.; Yazyev, O.; Austin, A. J.; Cammi, R.; Pomelli, C.; Ochterski, J. W.; Martin, R. L.; Morokuma, K.; Zakrzewski, V. G.; Voth, G. A.; Salvador, P.; Dannenberg, J. J.; Dapprich, S.; Daniels, A. D.; Farkas, O.; Foresman, J. B.; Ortiz, J. V.; Cioslowski, J.; Fox, D. J. *Gaussian 09*, revision A.02; Gaussian, Inc.: Wallingford, CT, 2009.

(43) Paulus, E. F.; Leusen, F. J. J.; Schmidt, M. U. Crystal structures of quinacridones. *CrystEngComm* **2007**, *9*, 131−143.

(44) Mei, X.; Wolf, C. Crystallization through Slow Acid-Controlled Hydrolytic Release of a Highly Polar Organic Compound: Formation of a Dipolar Acridone Polymorph. *Cryst. Growth Des.* **2005**, *5*, 1667−1670.

(45) Dzyabchenko, A. V.; Zavodnik, V. E.; Bel'skii, V. K. *Kristallografiya* **1980**, *25*, 72.

(46) Rovira, C.; Veciana, J.; Santaló, N.; Tarrés, J.; Cirujeda, J.; Molins, E.; Llorca, J.; Espinosa, E. Synthesis of Several Isomeric Tetrathiafulvalene π-Electron Donors with Peripheral Sulfur Atoms. A Study of Their Radical Cations. *J. Org. Chem.* **1994**, *59*, 3307−3313.

(47) You, J.; Zhao, H.; Sun, Z.; Xia, L.; Yan, T.; Suo, Y.; Li, Y. Application of 10-ethyl-acridine-3-sulfonyl chloride for HPLC determination of aliphatic amines in environmental water using fluorescence and APCI-MS. *J. Sep. Sci.* **2009**, *32*, 1351−1362.

(48) Huang, P.-C.; Parthasarathy, K.; Cheng, C.-H. Copper-Catalyzed Intramolecular Oxidative C-H Functionalization and C-N Formation of 2-Aminobenzophenones: Unusual Pseudo-1,2-Shift of the Substituent on the Aryl Ring. *Chem. - Eur. J.* **2013**, *19*, 460−464.

(49) Sharma, B. K.; Shaikh, A. M.; Agarwal, N.; Kamble, R. M. Synthesis, photophysical and electrochemical studies of acridone-amine based donor−acceptors for hole transport materials. *RSC Adv.* **2016**, *6*, 17129−17137.

(50) Sheldrick, G. M. Crystal structure refinement with *SHELXL*. *Acta Crystallogr., Sect. C: Struct. Chem.* **2015**, *C71*, 3−8.

DOI: 10.1021/acs.joc.8b02939